

Nonlinear Viscoelasticity and the Formation of Transverse Ridges

DAVID BERCOVICI

Department of Geology and Geophysics, University of Hawaii, Honolulu

HENRY J. B. DICK

Department of Geology and Geophysics, Woods Hole Oceanographic Institution, Woods Hole, Massachusetts

THOMAS P. WAGNER

Department of Earth, Atmospheric and Planetary Sciences, Massachusetts Institute of Technology, Cambridge

Transverse ridges are regions of anomalously high uplift that run parallel to many of the transform faults at mid-ocean ridges. Previous models of the formation of these ridges generally fail to explain the magnitude of uplift (between 1 and 8 km) or account for geophysical observations (which indicate that the ridges are dynamically uplifted by neutral or heavy, but not buoyant, material). However, the potentially large Maxwell relaxation time of the lithosphere and the high strain rates and finite deformation of transform faults imply that nonlinear viscoelasticity may play an important role in the formation of these ridges. We present simple theoretical and experimental models of viscoelastic flow beneath a transform fault to show that the purely horizontal motion of the fault can generate vertical uplift typical of transverse ridges. The theoretical model is of an infinite half-space of fluid driven from above by two plates moving parallel and in opposite directions to one another. The constitutive relation for the viscoelastic rheology is for a second-order fluid; i.e., nonlinear viscoelastic effects are treated as perturbations to Newtonian, purely viscous flow. The theoretical model not only predicts the two transverse ridges that are often observed on either side of the transform fault, but the central transform valley that separates them as well. For typical lithospheric flexural rigidity and deformation associated with transverse ridges, the viscoelastic effect provides sufficient vertical stress to produce the observed uplift. Further, the dynamic uplift is a purely mechanical effect (i.e., it does not involve buoyant material) which corresponds to geophysical observations. The experimental model is comprised of a viscoelastic fluid (2% aqueous solution of high molecular weight carboxymethylcellulose) driven by a rotating plate. This is analogous to a transform fault because the boundary of a spinning circular tectonic plate (surrounded by stationary plates) is one continuous transform fault. The experiment produces a large ridge of fluid along the edge of the plate with a slight trough outside of the ridge; this result is qualitatively described by a cylindrical version of the above theoretical model. In conclusion, both experimental and theoretical models show that when nonlinear viscoelasticity is accounted for, uplift characteristic of transverse ridges can be generated from purely horizontal motion typical of transform faults.

INTRODUCTION

Transverse ridges are an enigmatic feature of the Earth's mid-ocean spreading centers. They are relatively narrow zones of extreme uplift, with peaks ranging between 1 and 8 km above the seafloor, flanking many oceanic transform faults (Figures 1a and 1b). Rocks along these ridges may be elevated from beneath the seafloor to above the sea surface to form islets such as St. Paul's Rocks near St. Paul's Fracture Zone in the equatorial Atlantic Ocean [Melson and Thompson, 1971]; other instances of uplift to sea level are suggested by wave cut platforms and coral reefs, such as at the Romanche Fracture Zone in the Atlantic [Bonatti and Honnorez, 1971, 1976; Honnorez et al., 1975; Bonatti and Chermak, 1981; Bonatti et al., 1983; Fisher and Sclater, 1983; Dick et al., 1990].

Previous models of the formation of these ridges (see below) do not accord with either the total amount of uplift or geophysical observations. The high strain rates (i.e., compared with typical geodynamic strain rates) and finite de-

formation across the transform faults, along with the large lithospheric Maxwell relaxation time (i.e., a characteristic time for elastic stresses to be relaxed away by viscous flow), have led us to consider a new model concerning the purely mechanical effects of nonlinear viscoelasticity. We show with relatively simple theory and a laboratory experiment that nonlinear viscoelasticity can turn the horizontal motion of transform faults into vertical uplift that (in shape, size, and correlation with observations) is highly suggestive of transverse ridges.

Transverse Ridges: Geological Observations

Transverse ridges generally occur or are most pronounced at slow spreading centers (e.g., the Mid-Atlantic Ridge with spreading velocities of the order of 1 cm/yr). These ridges can appear on both sides of the transform fault (as at the Romanche Fracture Zone) or one side of the fault (e.g., the Vema Fracture Zone in the Atlantic Ocean) (Figure 1b). At slow spreading centers, there is typically also a central transform valley centered along the transform fault. The valley is typically 4 to 5 km deep in relation to normal seafloor, with the greatest depths along the active transform fault occurring in the nodal basins located at or near the ridge-transform intersection.

Copyright 1992 by the American Geophysical Union.

Paper number 92JB00890.
0148-0227/92/92JB-00890\$05.00

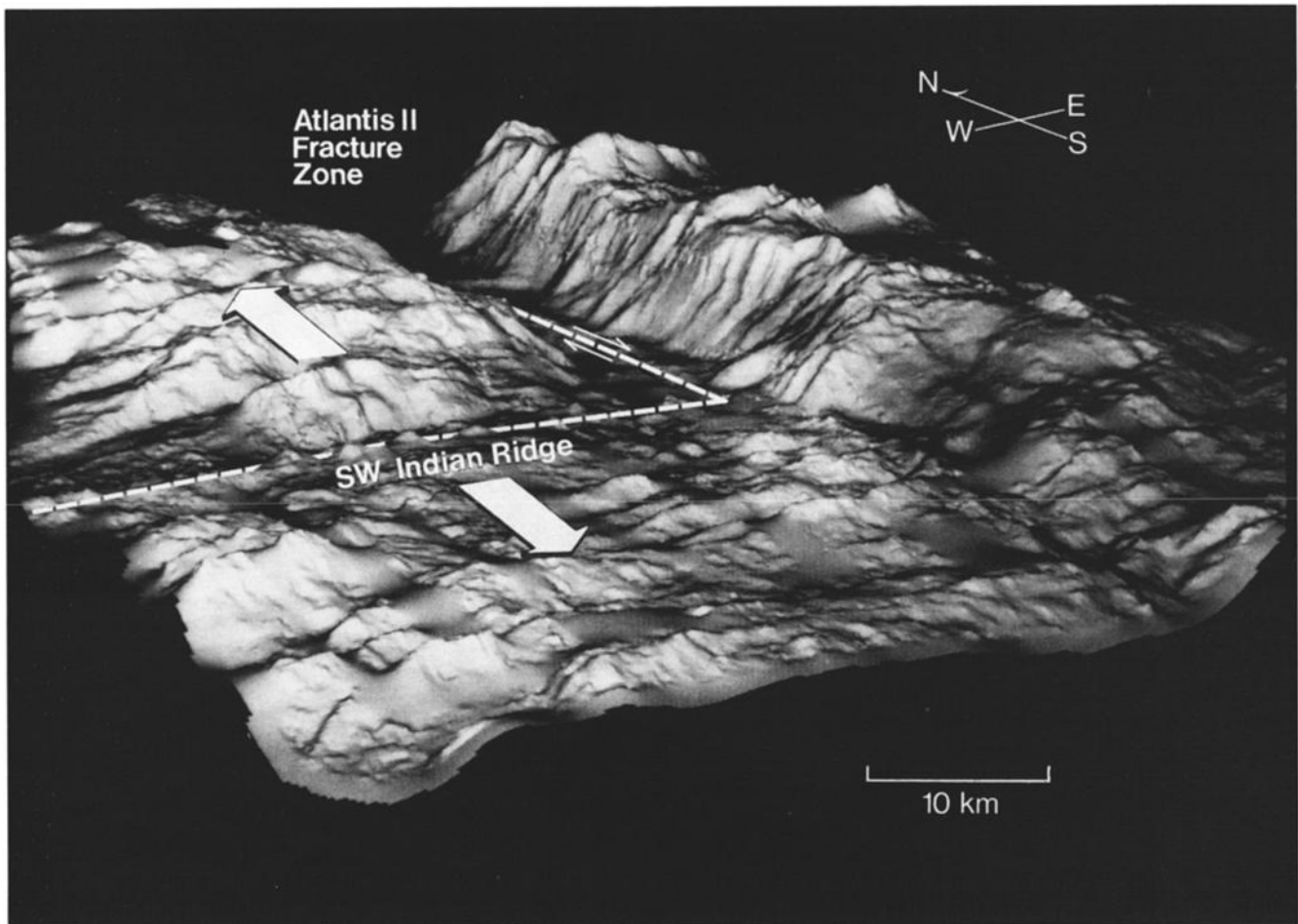


Fig. 1a. A three-dimensional bathymetric image, made from high-resolution Sea Beam data, of the transverse ridges flanking the central transform valley at the Atlantis II Fracture Zone in the Indian Ocean.

While oceanic fracture zones typically extend beyond the active transform fault region into the plate interiors (thereby marking the paleotrace of the transform), transverse ridges generally do not. The opposing walls of the fracture zone valley in these inactive fracture zones have very different origins: one wall having passed through the transform tectonic zone, while the other has not. Transverse ridges, common on transform and paleotransform walls, are generally absent along nontransform walls. Thus the origin of the ridges is possibly linked to the shearing motion along transform faults.

Transverse ridges themselves may be continuous (e.g., at the Vema Fracture Zone) or a series of undulations along the length of the ridge (e.g., the Kane Fracture Zone in the North Atlantic). Where the rift valley of the spreading center and the transform walls intersect, there is frequently great uplift, forming what is known as an "inside corner high" which can extend above sea level (e.g., St. Paul's Rocks) [Melson and Thompson, 1971; Searle and Laughton, 1977; Karson and Dick, 1983; Fox and Gallo, 1984; Sevringhaus and Macdonald, 1988]. The abundant exposure of plutonic rocks, particularly mantle peridotites, over large regions along the lengths and crests of many of these ridges indicates unusual tectonic processes not occurring at the adjacent mid-ocean spreading centers [Dick et al., 1990].

Previous Models

Since the first observation of transverse ridges, several models have been developed to explain their presence, morphology, and anomalous uplift. One of the earliest models developed to explain the formation of the nodal basin involves viscous head loss of a conduit (or sheet) of fluid passively upwelling along a spreading center [Sleep and Biehler, 1970]; i.e., the conduit maintains a negative hydraulic head at the surface and thus a pressure low to sustain flow from the asthenosphere into the conduit (in other words, the spreading motion generates a suction force in the conduit so that the conduit can be replenished). The negative hydraulic head creates the rift valley along the spreading center and is enhanced at the transform fault-spreading center intersection (because additional material is being drawn from the conduit into the transform fault, thus a larger pressure low is required to feed the conduit) to form the nodal basin. Material carried out of the pressure low rebounds to hydrostatic equilibrium, creating the uplifted blocks on the rift valley walls and the transverse ridges themselves. This implies that the transverse ridges are isostatically supported and are thus normal crust that only appear to be ridges by virtue of contrast with the central transform valley and nodal basin. This would then imply that the ridges should essentially be of the same elevation as the rift valley walls;

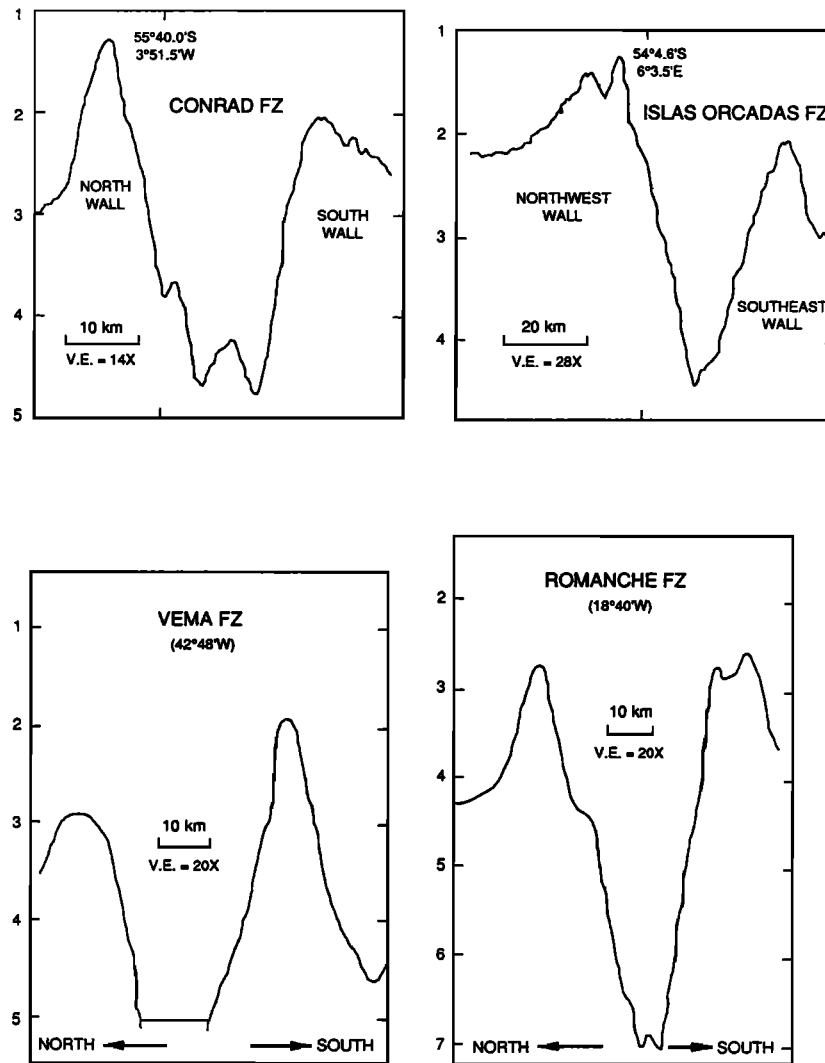


Fig. 1b. Cross-sectional profiles of the transverse ridge systems at the Conrad and Islas Orcadas fracture zones in the southwest Indian Ocean [Slater *et al.*, 1978] and the Vema and Romanche fracture zones in the Equatorial Atlantic [Bonatti and Honnorez, 1976].

as transverse ridges rise in some instances to sea level, this mechanism is probably not adequate to explain the formation of the ridges.

Based on the frequent exposure of serpentinized peridotite, which has a relatively low density compared with basalt, gabbro, or mantle, a number of authors have suggested that ongoing serpentinization of the mantle due to percolation of seawater down faults in the transform fault region would produce vertical uplift from both volume expansion and buoyancy caused by the reduction in density from hydration of mantle rock [Bonatti, 1978; Macdonald *et al.*, 1986; Dick *et al.*, 1990]. While this mechanism may account for the small median tectonic ridge along the floor of the central transform valley, it cannot account for the relief of the transverse ridges, the existence of the central transform valley, and the fact that the ridges consistently flank the transform fault and the central transform valley. Furthermore, both this mechanism and that of viscous head loss suggest that the ridges are isostatically supported. However, examination of the gravity field over transverse ridges at the Kane, Romanche, and Vema fracture zones in the At-

lantic and the Atlantis II Fracture Zone in the Indian Ocean [Cochran, 1973; Robb and Kane, 1975; Loudon and Forsyth, 1982; J. Snow, personal communication, 1990] shows that these ridges are not only dynamically (i.e., nonisostatically) supported but are compensated at depth by heavy, not buoyant, material; i.e., although uplift is dynamic, it is not from buoyancy forces. Seismic refraction studies of these ridges have been hindered by the rough terrain and extreme relief, but what little data are available concur with the gravity data [Detrick and Purdy, 1980; Abrams *et al.*, 1988]. Thus mechanisms involving isostatic compensation or dynamic support from buoyant material are more or less precluded by the available data.

One possible nonisostatic, nonbuoyant mechanism for the formation of transverse ridges is lithospheric buckling under compressional stresses, augmented by thermal bending moments, across transforms [Wessel, 1990]. Plate reconstructions of many fracture zones, however, demonstrate that transient changes in spreading direction caused the transform faults to undergo extension during the formation of large transverse ridges [Tucholke and Schouten, 1988; Dick

et al., 1990]. Although lateral density variations across the fracture zone [Bonatti, 1978] can also cause uplift near a transform fault, they generally cannot induce the observed large relief.

In summary, a successful model of the formation of transverse ridges should involve dynamic, yet nonbuoyant, uplift of the oceanic lithosphere near transform faults. In the remainder of this paper, we present a new model based on nonlinear viscoelastic deformation that satisfies these requirements in addition to generating the requisite topography.

VISCOELASTICITY

Viscoelastic deformation occurs when a medium undergoes irrecoverable (viscous) deformation yet still has memory of past (elastic) deformations. Viscoelasticity is less a material property than a characteristic of the time scale over which deformations occur. The relevance of viscoelasticity is determined by the ratio of the Maxwell relaxation time t_r to the typical time scale for deformations, or fluid flow, to occur t_f ; this ratio is the Deborah number $De = t_r/t_f$ [Bird et al., 1987]. The Maxwell relaxation time $t_r = \eta/\mu$ (where η is a characteristic dynamic viscosity and μ is an elastic modulus, typically the modulus of rigidity) is the characteristic time for the relaxation of elastic stresses by viscous flow (i.e., stresses decay as e^{-t/t_r}). The flow time scale t_f is determined by the velocities and geometry of the deforming medium; e.g., fluid flowing at a maximum velocity v in a channel of width d has a time scale of deformation $t_f = d/v$; thus t_f can also be considered the inverse of the characteristic strain rate. For $De \ll 1$, elastic stresses are relaxed away much faster than the medium is deforming and hence the flow is almost purely viscous; this is typically the case in most geodynamic settings, such as mantle convection. Alternatively, for $De \gg 1$, the medium behaves as an elastic. Viscoelastic behavior occurs when De is neither $\ll 1$ nor $\gg 1$. In the Earth sciences, viscoelastic behavior is primarily only treated when estimating the viscosity (and postglacial structure) of the Earth's mantle from data on the postglacial rebound of high-latitude continental bodies [Cathles, 1975; Peltier, 1982; Yuen et al., 1982]. At transform faults, $t_r = 10^4$ – 10^7 years (based on material properties of the oceanic lithosphere) [Beaumont, 1976; Watts et al., 1982; De Bremaecker, 1985], which can be much larger than the value of t_r for the Earth's mantle because the lithosphere is relatively cold and has a very high viscosity. The flow or deformation time scale t_f is typically the inverse shear strain rate across the transform fault; thus t_f is typically 10^5 – 10^6 years [Fox and Gallo, 1984]. (We show a posteriori that t_f is based on the strain rate across the fault and not another time scale.) Therefore the Deborah number for transform faults can be of the order of 1 or greater, implying that where continuous deformation occurs near the faults, viscoelastic effects may be considerable.

The classical treatment of viscoelasticity in geophysics is for linear viscoelasticity. This is usually modeled as a combination of elastic springs and viscous dashpots which lead to constitutive stress-strain relations involving partial time derivatives only (the strain rate, however, is the full and not the partial time derivative of the strain) [Bird et al., 1987; Turcotte and Schubert, 1982]. A typical viscoelastic model is the Maxwell body with an elastic spring and a viscous dashpot in series; this leads to the constitutive rela-

tion $\tau + t_r \partial \tau / \partial t = 2\eta \dot{\epsilon}$, where τ is a one-dimensional stress (and thus a scalar) and $\dot{\epsilon}$ is the one-dimensional strain rate. Since the instantaneous strain rate $\dot{\epsilon}$ is the same for both linear and nonlinear viscoelastic theories, it is kept distinct from other time rates of change. This theory is only valid in the limit of infinitesimal deformation, or strain, and thus is called linear since the constitutive relation is linearized.

When deformation is finite, as it is along transform faults, it is necessary when treating viscoelasticity to consider finite relative strain, which is a nonlinear function of the displacement gradients [Malvern, 1969]. This leads to a nonlinear constitutive relation in which the partial time derivatives of stress and strain rate from linear theory are replaced by convective time derivatives [Bird et al., 1987]; e.g., $\partial \underline{\tau} / \partial t$ in the constitutive relation for the Maxwell body is replaced by

$$\frac{D\underline{\tau}}{Dt} - \{(\nabla \underline{v})^t \cdot \underline{\tau} + \underline{\tau} \cdot (\nabla \underline{v})\} \quad (1)$$

where $\underline{\tau}$ is the stress tensor, \underline{v} is the velocity vector, $D/Dt = \partial/\partial t + \underline{v} \cdot \nabla$ is the material derivative, and $(\nabla \underline{v})^t$ is the transpose of the velocity gradient tensor $(\nabla \underline{v})$. Equation (1) is the contravariant convective time derivative of $\underline{\tau}$; other convective derivatives are also possible [Bird et al., 1987]. Physically, the convective derivative represents the time rate of change and advection of the stress or strain rate fields (the D/Dt term) and the rotation and deformation of these fields by the flow (the $\{..\}$ term).

Nonlinear viscoelastic effects are well documented in the field of polymeric fluid dynamics. For the purposes of this paper, the most important, and perhaps well known, are "rod-climb" [Garner and Nissan, 1946], the Quelleffekt [Böhme et al., 1985], and the secondary flow in a disk-cylinder configuration [Kramer and Johnson, 1972; Hill, 1972; Nirschl and Stewart, 1984]. Rod-climb occurs when a spinning rod is placed in a polymeric fluid: instead of fluid spinning away from the rod under centrifugal acceleration, it moves in toward and climbs up the rod. The Quelleffekt is a similar phenomenon wherein a disk spinning at the base of a cylinder of polymeric fluid causes the surface of the fluid to be deflected upward at the axis of the disk and downward at the walls of the cylinder. The secondary flow in a disk-cylinder configuration is virtually identical to the Quelleffekt: a disk spinning on top of a cylinder of polymeric fluid creates a secondary flow with a downward jet along the disk axis and upwelling at the cylinder walls, opposite in sense to what would be caused by centrifugal effects in a Newtonian fluid. It is easy to see that when the secondary flow is turned upside down, it will cause the Quelleffekt. An adaptation of the disk-cylinder experiment is in fact used for our experimental model. From an intuitive approach, these effects are essentially due to the elastic components of the fluid winding around the axis of the rotor (analogous to rubber bands winding around a spinning shaft), creating an inward tension which results in vertical stress (by the inward squeezing of the fluid) and hence uplift in the rod-climb experiments and the Quelleffekt, and the secondary flow in the disk-cylinder experiment. For a review of these effects and more, see Bird et al. [1987].

Nonlinear viscoelastic effects have also been considered in several geophysical contexts, such as glacial flows [McTigue et al., 1985; Man and Sun, 1987] as well as landslides and

granular flows [Savage, 1984]. In these studies, nonlinear viscoelastic effects are referred to as normal stress effects because of the fact that nonlinear viscoelasticity allows normal stresses to arise from shear flows.

Finally, it should be emphasized that there is no known, unique viscoelastic rheology, linear or nonlinear, for the Earth's lithosphere and mantle. We argue that nonlinear viscoelastic effects may be important at transverse ridges because (1) the Maxwell relaxation time of the lithosphere is possibly quite large, (2) the deformation time scales of transform faults are quite small, and (3) deformation at transform faults is finite; the argument is based on time scales and on amplitude of deformation, not on any specific rheology. Thus the theoretical and experimental work presented here comprises an idealized investigation of viscoelastic effects as they might occur beneath transverse ridges, but they do not represent a rigorous model of oceanic lithosphere near a transform fault. The models will account for normal stresses generated through nonlinear viscoelasticity, but not for the effects of temperature- and stress-dependent viscosities that are normally associated with lithospheric material. In this respect, it is important to note that under the strain rates near a transform fault, the effective viscosity of the viscously deforming lithosphere may be much lower than the surrounding, less rapidly deforming lithosphere because of non-Newtonian pseudo-plastic behavior and/or shear heating [Schubert and Turcotte, 1972; Forsyth and Uyeda, 1975]. These effects would tend to diminish the importance of viscoelastic behavior by reducing De . For this present simple analysis, we will not consider the effects of variable viscosity beneath the transform fault, although such effects must be noted when drawing conclusions from our simple models.

THEORETICAL MODEL

The Second-Order Fluid and Other Assumptions

Viscoelastic fluids are known to exhibit fairly exotic flows; hence a rigorous theoretical model of nonlinear viscoelastic deformation would invariably require an involved numerical calculation. However, for a first analysis, we use a theoretical model that is greatly simplified to facilitate a straightforward analytic solution. The constitutive relation we employ is for a second-order fluid [Bird et al., 1987]:

$$\underline{\tau} = 2\eta(\underline{\dot{\epsilon}} + \lambda_1 \left[\frac{D\underline{\dot{\epsilon}}}{Dt} - (\nabla \underline{v})^\dagger \cdot \underline{\dot{\epsilon}} - \underline{\dot{\epsilon}} \cdot (\nabla \underline{v}) \right] + 2\lambda_2 \underline{\dot{\epsilon}} \cdot \underline{\dot{\epsilon}}) \quad (2)$$

where $\underline{\dot{\epsilon}} = \frac{1}{2}(\nabla \underline{v} + (\nabla \underline{v})^\dagger)$ is the strain rate tensor, and λ_1 and λ_2 are retardation time constants. (Retardation time constants are analogous to t_r , except that they measure the retardation of a viscoelastic material's response to an instantaneous stress instead of relaxation of stress after an instantaneous strain; the retardation effect is characterized by the Kelvin-Voigt body in linear viscoelasticity; see Turcotte and Schubert [1982].) It can be shown from continuum mechanics considerations that $\lambda_1 < 0$ and from molecular theories that λ_2 is also typically negative for an undiluted system of polymers [Bird et al., 1987]. A first-order fluid ($\lambda_1 = \lambda_2 = 0$) would simply be a Newtonian viscous fluid; thus (2) contains the lowest order viscoelastic perturbation to purely viscous flow. The second-order fluid approximation and higher-ordered approximations are

closely related to the Rivlin-Ericksen expansions; for an outline of the derivation of the ordered fluid approximation or Rivlin-Ericksen expansions, see Tanner [1985, p. 133].

A second-order fluid is a significant simplification, and thus there are several limitations to its applicability. It leads to spurious instability in unsteady flows and is not a good approximation for flows around sharp corners [Tanner, 1985]. Also, since it is a perturbation expansion around a Newtonian viscous constitutive equation, it is only valid for small De .

If we set $\lambda_1 = \lambda_2 \equiv \lambda$, we can exploit the three-dimensional flow theorem of Giesekus [Giesekus, 1963] which states that a velocity field that satisfies the Newtonian, incompressible equation for Stokes (i.e., creeping) flow also satisfies the equation for Stokes flow of an incompressible second-order fluid; the pressures and stresses of the Newtonian and second-order fluids, however, will be different. We can therefore calculate a Newtonian flow field and determine the resultant nonlinear viscoelastic stress without necessarily determining any secondary flow. However, we must note that our assumption that $\lambda_1 = \lambda_2 = \lambda < 0$ cannot be rigorously justified; this emphasizes the importance of performing laboratory experiments (discussed in the following section) to empirically test the validity of our assumptions.

As an aside, we note that it is not, in fact, necessary for $\lambda_1 = \lambda_2$ for the Newtonian and second-order fluids to have the same velocity field. The rectilinear flow theorem of Langlois, Rivlin, and Pipkin [Pipkin and Rivlin, 1963; see Bird et al., 1987] also specifies that the two fluids will have the same flow field if the only nonzero component of the Cartesian velocity vector $\underline{v} = (u, v, w)$ is $u(y, z)$, $v(x, z)$, or $w(x, y)$, even when λ_1 and λ_2 are independent of one another. However, in the final analysis, the stresses proportional to λ_1 are not used in our problem; thus it is irrelevant which theorem we use.

Given the above assumptions and approximations, our basic methodology is to (1) calculate the velocity field for a Newtonian constant viscosity fluid beneath an idealized transform fault, (2) use this velocity to calculate the non-Newtonian viscoelastic stresses from equation (2), and (3) use these viscoelastic stresses to determine the vertical uplifting stress beneath the transform fault.

Newtonian Viscous Flow Beneath a Transform Fault

Our theoretical model configuration of a transform fault is comprised of two plates moving parallel and in opposite directions to one another over an infinite half-space of fluid (Figure 2). The inner and outer edges of the two plates are separated by a distance $2l$ and $2L$, respectively. The region of width $2l$ separating the plates represents the shear zone of the transform fault. We assume that the velocity everywhere is only in the direction of the plates' motion, the y direction, and is only a function of depth z and distance x perpendicular to the shear zone (the centerline of the shear zone is at $x = 0$). We also assume that the velocity v_0 at the surface $z = 0$ is a function of x :

$$v_0(x) = \begin{cases} -V & -L \leq x \leq -l \\ Vf(x) & -l \leq x \leq l \\ V & l \leq x \leq L \end{cases} \quad (3)$$

The function $f(x)$ is one of two simple functions. For the first $f(x) = f_1(x)$ we assume that $l \ll L$, and thus velocity

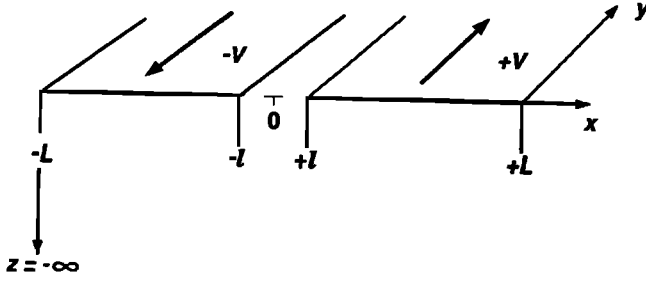


Fig. 2. Schematic diagram of the theoretical model. See text for discussion.

varies linearly with x between the plates; i.e., $f_1(x) = x/l$. However, this velocity profile creates discontinuities in velocity gradients which the second-order fluid approximation is poor at resolving. Thus to insure that such discontinuities do not cause spurious effects, we also try a smooth function; i.e., $f(x) = f_2(x) = \frac{1}{2}(3x/l - x^3/l^3)$.

The Stokes equation (i.e., the force balance equation for creeping flow) for an incompressible, constant viscosity Newtonian fluid without body forces is

$$0 = -\nabla P + \eta \nabla^2 \underline{v} \quad (4)$$

where P is the nonhydrostatic pressure. For flow in the y direction, where there is no y dependence, this equation is simply the two-dimensional harmonic equation for the y component of the velocity v :

$$\frac{\partial^2 v}{\partial x^2} + \frac{\partial^2 v}{\partial z^2} = 0 \quad (5)$$

With the boundary conditions $v(x, z) = v_0(x)$ at $z = 0$ and v is finite as $z \rightarrow -\infty$, the solution for v is

$$v(x, z) = \sum_{n=1}^{\infty} \frac{2V}{n\pi} [b_n(\epsilon) - \cos(n\pi)] \sin(n\pi x/L) e^{n\pi z/L} \quad (6a)$$

where

$$b_n(\epsilon) = \begin{cases} \frac{\sin(n\pi\epsilon)}{n\pi\epsilon} & f(x) = f_1(x) \\ \frac{3}{(n\pi\epsilon)^2} \left[\frac{\sin(n\pi\epsilon)}{n\pi\epsilon} - \cos(n\pi\epsilon) \right] & f(x) = f_2(x) \end{cases}, \quad (6b)$$

$\epsilon = l/L$ and we have assumed that $v_0(x)$ is periodic with period $2L$. Equation (6) reduces to the Fourier series for a step function (i.e., $b_n(\epsilon) \rightarrow 1$) in the limit $\epsilon \rightarrow 0$. This purely horizontal velocity field will be used to calculate the vertical uplift due to viscoelastic stresses.

Viscoelastic Vertical Stresses

An equation for the total vertical stresses at the surface of the fluid is obtained by adding $\partial \tau_{zz} / \partial x$ (where τ_{ij} is the component of stress acting in the j direction on surfaces facing in the i direction) to both sides of the x component of the Stokes flow equation (written in terms of stresses and independent of y):

$$0 = -\frac{\partial P}{\partial x} + \frac{\partial \tau_{xx}}{\partial x} + \frac{\partial \tau_{xz}}{\partial z} \quad (7)$$

and rearranging:

$$\frac{\partial}{\partial x}(P - \tau_{zz}) = \frac{\partial}{\partial x}(\tau_{xx} - \tau_{zz}) + \frac{\partial \tau_{xz}}{\partial z} \quad (8)$$

The total vertical stress $P - \tau_{zz}$ causes uplift at the surface, and the amount of uplift depends on the surface's flexural

rigidity. For example, if the surface is free (i.e., no flexural rigidity), then the vertical stress causes a hydrostatic head; i.e., by continuity of vertical stress across $z = 0$, $\Delta \rho g h = P - \tau_{zz}$, where $\Delta \rho$ is the density contrast between the fluid and overlying medium, g is gravity, h is the height of the uplift above the surface, and we have assumed that the overlying medium is inviscid.

Proceeding, we use (2) (assuming steady state) with $\lambda_1 = \lambda_2 = \lambda < 0$ to calculate the stress components τ_{xx} , τ_{zz} , τ_{xz} in terms of the velocity v ; these we insert into (8). The indefinite integral of (8) over x (with the integration constant taken to be zero such that there is no net or mean uplift) yields an equation for the vertical stress:

$$P - \tau_{zz} = -|\lambda| \eta \left[\left(\frac{\partial v}{\partial x} \right)^2 - \left(\frac{\partial v}{\partial z} \right)^2 + \int \frac{\partial}{\partial z} \left(\frac{\partial v}{\partial x} \frac{\partial v}{\partial z} \right) dz \right] \quad (9)$$

With (6) substituted for v , we evaluate (9) at the surface $z = 0$, and after some algebra, we arrive at an expression for the dimensionless uplifting stress at the surface:

$$\left. \frac{P - \tau_{zz}}{|\lambda| \eta (V/l)^2} \right|_{z=0} = -2\epsilon^2 \sum_{n=1}^{\infty} \sum_{m=1}^{\infty} B_n(\epsilon) B_m(\epsilon) \times \left\{ \cos[(n+m)\pi x/L] - (1 - \delta_{nm}) \frac{n+m}{n-m} \cos[(n-m)\pi x/L] \right\} \quad (10)$$

where $B_n(\epsilon) = b_n(\epsilon) - \cos(n\pi)$. When written in the manner of (10), the nondimensional uplift is relatively insensitive to ϵ . Note that if $|\lambda| \equiv t_r = \eta/\mu$, then $|\lambda| \eta (V/l)^2 = \mu D e^2$, which implies that a De defined in terms of the strain rate across the transform fault is the relevant Deborah number for this problem. (We might just as easily have nondimensionalized $P - \tau_{zz}$ by $|\lambda| \eta (V/l)^2$; but then, since the right side of (10) is insensitive to ϵ , the amplitude of the dimensionless uplift would be proportional to ϵ^{-2} , and this would again verify that the width of the shear region determines the magnitude of the viscoelastic stresses.)

When (10) is plotted versus x/l (Figure 3), the curves are functions of ϵ only. However, the curves in fact vary only slightly in amplitude and shape with ϵ (for a given $b_n(\epsilon)$ defined in (6b)); thus they are essentially representative of uplift for any value of ϵ . For the linear shear zone (i.e., $f(x) = x/l$ in dimensionless units), two sharp ridges are predicted to occur at the inner boundaries of the plates, and these ridges are separated by a smooth valley. For the smooth shear zone (i.e., $f(x) = \frac{1}{2}(3x/l - x^3/l^3)$), two ridges separated by a valley again occur; yet the ridges are not sharp peaks, which insures that the uplift is not a spurious effect of velocity-gradient discontinuities. Comparing the two curves of Figure 3, one can see that the sharpness and amplitudes of the ridges are partially determined by the velocity gradients in the vicinity of $x = \pm l$. This implies that the ridges can be asymmetric across the shear zone if the velocity gradients are different at $x = -l$ and $x = l$.

A physical understanding of how the ridges and troughs form can be gained by considering the direction of elastic stresses in the vicinity of the model transform fault. Both viscous and elastic stresses oppose the motion of the plates; yet the elastic stress also has a component of tension perpendicular to the plate motion. This can be seen by imagining a rubber band at some angle θ to the plate edges (either

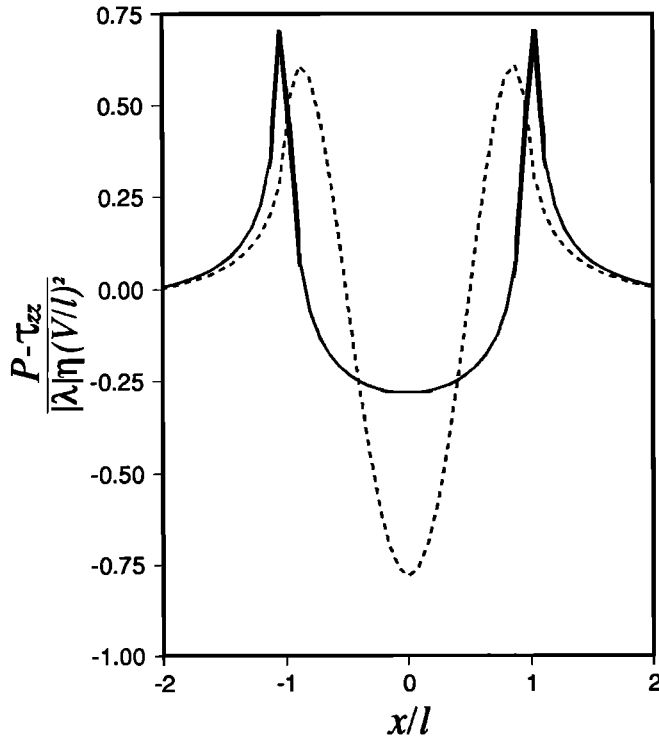


Fig. 3. Nondimensional uplift (in terms of vertical stress) versus nondimensional distance x/l (such that the shear zone always occurs in the region $-1 \leq x/l \leq +1$) for the theoretical model with $\epsilon = 0.25$ and a velocity profile across the shear zone at the surface that is either linear (solid line) or smooth (dashed line). In both cases, the series solution of (10) is truncated at $n, m = 500$, whereas the series converges for $n, m \geq 200$.

in or out of the plane of the plates) being stretched by the shearing motion such that it has tension T along its length. The elastic stress opposing the plate motion is $T \cos \theta$, and the tension perpendicular to the plate edges is $T \sin \theta$. The latter tension exerts a stress on the fluid directed perpendicular to the plate edges; this tension can drive fluid flow at right angles to the direction of plate motion. For example, vertical shear $\partial v / \partial z$ stretches a hypothetical rubber band dipping down into the fluid, causing a vertical tension which pulls fluid upward. Similarly, horizontal elastic tension across the fault (induced by horizontal shear $\partial v / \partial x$ stretching a rubber band placed across the fault) drives convergent flow toward $x = 0$ and thus a downwelling motion (or equivalently a pressure low), with subsequent downward deflection, occurs at $x = 0$.

However, not all the elastic tensions induced by the various shearing motions contribute equally to the net uplifting stresses. Close examination of the three terms on the left side of (9) shows that the second term (proportional to τ_{zz} or $(\partial v / \partial z)^2$) is primarily responsible for the shape and amplitude of the uplift; this term represents the vertical stress induced by the stretching of the elastic component of the fluid under vertical shear. The other terms make a smaller contribution to the net stress: the first term on the right side (τ_{xx}) enhances the trough between the peaks, while the third term reduces the amplitudes of both the trough and peaks but is much smaller than the first two terms. Therefore the lateral variation in uplift leading to the ridge-valley-ridge surface morphology is primarily due to lateral variation in the vertical shear. This lateral variation occurs

because v decays with depth within a characteristic length proportional to the horizontal wavelength of the surface velocity field (see (6)). Far from the fault, the surface velocity field is smooth, hence the dominant horizontal wavelength is large; in the vicinity of the fault, the velocity field has a horizontal wavelength characteristic of the fault width. Therefore the velocity field decays much more rapidly with depth beneath the fault than far from the fault (physically, because the high strain rates beneath the fault are much harder for the fluid to support), leading to a larger absolute value of $\partial v / \partial z$ (and thus greater vertical elastic tension) in the vicinity of the fault. The trough occurs because the vertical shear goes to zero at the fault itself (i.e., $x = 0$) since $v = 0$ there. Therefore the maximum vertical shear (and thus the maximum vertical elastic stress) occurs near the fault but not on the fault itself where there is a local minimum in $|\partial v / \partial z|$; since the system is symmetric about the fault (i.e., the results of this analysis should not depend on whether we are looking up or down the strike of the fault), there must be two identical maxima in $|\partial v / \partial z|$ on either side of the fault and thus two symmetric peaks. This physical explanation is lacking, however, because it implies a secondary flow while the above theory does not account for secondary flow. However, later we will see that the second-order fluid theory essentially predicts the uplift as if there were secondary flow.

Induced Uplift and Lithospheric Flexure

To compare the theoretical results with geophysical observations, we first determine what stresses are approximately necessary to generate the observed uplift of a transverse ridge. We first assume that in the region of the fault itself $-l \leq x \leq l$, the lithosphere is comprised of highly sheared and loose material of little or no flexural rigidity. In this region, the downwarping leading to the transform valley merely results from hydrostatic compensation of the downward viscoelastic normal stresses. The more restrictive uplift occurs at the flanks of the fault zone, where the lithosphere is bent upward. For an order of magnitude calculation, we assume that the uplift of either flank of fault zone is due to a line load applied at the free edge of the plate. The relation between a line load W (units of newtons per meter) applied to the edge of a broken lithospheric plate and the resulting flexural uplift h is [Turcotte and Schubert, 1982, p. 127]

$$W = \Delta \rho g \alpha h \quad (11)$$

where $\Delta \rho$ is the density contrast between the mantle and overlying water and g is gravitational acceleration. The flexural wavelength α is given by

$$\alpha = \left[\frac{2\mu d^3}{3(1-\nu)\Delta \rho g} \right]^{1/4} \quad (12)$$

where d is the thickness of the lithospheric plate being bent and ν is Poisson's ratio. Using values of $\Delta \rho = 2300 \text{ kg/m}^3$, $g = 10 \text{ m/s}^2$, $\mu = 28 \text{ GPa}$, $\nu = 0.25$ [Turcotte and Schubert, 1982], and $d = 1 \text{ km}$ (for a characteristic lithospheric thickness near the ridge axis), we find that $\alpha = 5736 \text{ m}$; the typical uplift h for a transverse ridge is of the order of 1 km (though it may reach extremes of 8 km), for which we therefore require $W = 132 \text{ GPa m}$.

To relate the line load to the viscoelastic stress, we estimate W by calculating the area of the curve beneath one of the positive flanks on the normal stress curve (Figure 3). As either one of these flanks (for either the linear or smooth shear zones) is nearly a triangle, we approximate the line load by the relation

$$W = \frac{l}{2b} \max(P - \tau_{zz}) \quad (13)$$

where l/b is the base width of the triangle, and we estimate b to be 2.8 and 1.3 for the linear and smooth shear zones, respectively. (The base width is determined by fitting a triangle to either positive hump of the stress curve, truncating the tails that occur as $x \rightarrow \pm L$.) It should be noted that the line load approximation is best when $l/(2b) \ll \alpha$ and fails outright if $l/(2b) > \alpha$, as the flexural response to the normal stress $\max(P - \tau_{zz})$ would then be greater than the hydrostatic response (for which $\max(P - \tau_{zz}) = \Delta\rho gh$).

From Figure 3, the maximum stress is

$$\max(P - \tau_{zz}) = \hat{\sigma} \mu \left(\frac{\eta V}{\mu l} \right)^2 \quad (14)$$

where $\hat{\sigma}$ is 0.75 and 0.63 for the linear and smooth shear zones, respectively, and we have assumed that $|\lambda| = \eta/\mu$. For plate velocity, we use $V = 5$ cm/yr. Since viscosity undergoes orders of magnitude change across the lithosphere, it is unclear what the most appropriate choice is for viscosity η . The choice for the fault half-width l is also vague, as there is no well-defined shear zone and the observed geometry of the transverse-ridge systems is likely influenced by flexural damping. Thus we simply determine the viscosity necessary to generate the uplift $h = 1$ km (or line load $W = 132$ GPa m) for a range of fault widths in which $1 \text{ km} \leq l \leq 10 \text{ km}$. It should be noted that while the line load approximation is sufficient at $l = 1$ km, it worsens as $l \rightarrow 10$ km; yet, for all fault widths, $l/(2b) < \alpha$ if not $\ll \alpha$. For these fault widths, and the two shear zone cases, the necessary viscosity lies in the range $2 \times 10^{21} \text{ Pa s} \leq \eta \leq 1 \times 10^{22} \text{ Pa s}$, which are reasonable mantle viscosities. (Obviously, a change in plate velocity V by a factor c will change the limits of the viscosity range by a factor $1/c$, while a change in uplift h by a factor c' will change the limits by a factor $\sqrt{c'}$. Given the typical variability of V and h , the viscosity range is fairly robust.) Thus the viscoelastic mechanism can generate the requisite uplift given the available mantle and/or lower lithosphere viscosities. In fact, as there is, to our knowledge, no information about mantle viscosity inherent in the theoretical model or the above rough calculation, it is intriguing (or coincidental) that η should be so close to an actual mantle viscosity. However, it is by no means certain that the viscosity of the lithosphere beneath the fault is actually within or over the above range; as was mentioned previously, shear heating or non-Newtonian pseudo-plasticity may cause the effective viscosity to be well below this range.

One apparent inconsistency is that if the above viscosity range is assumed, excessive horizontal shear stress $\tau_{xy} \approx \eta V/l$ is generated beneath the fault. For the chosen velocity, viscosities and fault widths, the shear stress lies in the range $1 \text{ GPa} \leq \tau_{xy} \leq 5 \text{ GPa}$ while rocks undergo brittle failure at approximately 1 GPa [Ranalli, 1987]; for the viscoelastic mechanism to exist, the lithosphere must deform

viscously, not by discontinuous failure. However, given the approximate nature of the theoretical model and the uncertainty in the above flexure calculation, this inconsistency is marginal and does not necessarily preclude the viscoelastic mechanism. If sufficient viscoelastic uplift could occur with viscosities slightly less than the above range, such that $\tau_{xy} < 1$ GPa, then the lithosphere would, at worst, fail plastically (since the plastic yield stress is of the order of 100 MPa); since the medium would deform viscously after plastic failure (e.g., as in a Bingham model for a plastic fluid [Bird *et al.*, 1960]), there would be no inconsistency (at least with respect to shear stresses).

Finally, it is worth noting that for a constant line load, the uplift h decreases with plate thickness as $d^{-3/4}$. Thus even though the viscoelastic normal stresses of the theoretical model are symmetric across the fault and uniform along the fault, the uplift will diminish with lithospheric age and be asymmetric across the fault where there is an age offset, as is typically observed at transverse ridges.

EXPERIMENTAL MODEL

Because of the limitations of the second-order fluid approximation and to test the validity of assumptions made in our theoretical model, we have experimentally examined nonlinear viscoelastic uplift in a real fluid. However, it should be noted that neither the experimental test fluid nor Earth materials have precisely known or unique viscoelastic rheologies; thus there is not necessarily a real analogy between the test fluid and the Earth's lithosphere. The experiments described here are meant to demonstrate a rather general viscoelastic effect, i.e., the generation of normal stresses from simple shearing flow, and to verify that the theory does correctly describe viscoelastic behavior (at least qualitatively); they are not meant to represent a rigorous model of the Earth's lithosphere.

Our experimental model has a different configuration from that of the simple theoretical model presented above. The model is comprised of a disk of radius R_d spinning at angular frequency Ω on the surface of a viscoelastic fluid of depth H contained in a cylinder of radius R_c (Figure 4a). This model is analogous to a tectonic plate with a transform fault because the boundary of a spinning circular tectonic plate (surrounded by stationary plates) is one continuous transform fault. Thus the spinning disk model essentially isolates the plate's motion along the transform fault. (It could also be said that the rotating disk represents the purely rotational motion of fluid in the shear region $-l \leq x \leq l$ of the theoretical model.)

The viscoelastic fluid is comprised of a 2% aqueous solution of high molecular weight carboxymethylcellulose (CMC). (The exact CMC aqueous solution contains 220 g of dry CMC 7H3S [Aqualon Company, 1989] per 1 L of isopropyl alcohol, to suspend and disperse CMC particles prior to solution in water, per 10 L of distilled water.) CMC is a cellulose gum used in the cosmetics, foods, and pharmaceutical industries as an emulsion stabilizer and thickener. High molecular weight (or high viscosity) CMC at these concentrations is highly viscoelastic, which can be witnessed by its recoil after stirring. However, the long polymers that provide CMC with elasticity also cause its viscosity to be non-Newtonian shear thinning (because of the alignment of polymers in shear flow) over a certain regime of stress-strain

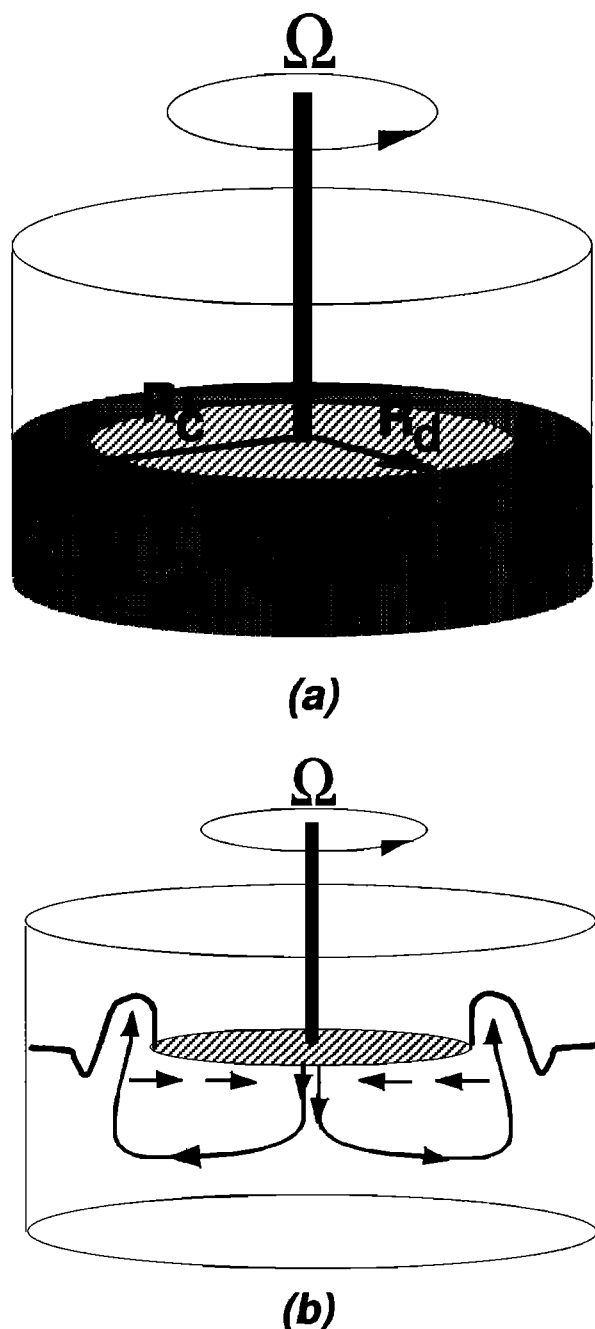


Fig. 4. (a) Schematic diagram of the disk-cylinder experimental apparatus and (b) a sketch of fluid motion in the experiment as inferred from particle motions. See text for discussion.

rate space. If the constitutive relation in the shear thinning regime obeys an Ostwald-de Waele (i.e., power law) model $\dot{\epsilon} \sim \tau^n$ (where shear thinning implies that $n > 1$), then n would be between 1.4 and 3 [Metzner, 1956]. The upper and lower asymptotes on viscosity as $\dot{\epsilon} \rightarrow 0$ and ∞ for a 1% solution are 2800 centipoise (cP) and 1000 cP, respectively; a 2% solution's viscosities are approximately a factor of 4 or 5 larger than these [Aqualon Company, 1989].

Approximately 10 L of the CMC solution are placed in a plexiglass cylindrical drum of radius $R_c = 12$ cm. A circular plastic disk attached to the shaft of a variable speed Bodine motor is lowered into the cylinder such that the disk rests on the surface of the fluid. The motor is spun up to its maximum revolutions per minute (rpm) to enhance coupling be-

tween the disk and fluid. This is necessary because at first the shear thinning property of CMC causes the disk and fluid to decouple. However, at high rpm, the normal upward stresses (due to viscoelastic uplift) build rapidly to a critical value where a secondary flow begins that couples a larger volume of fluid to the disk (by mixing high-momentum fluid with stationary fluid). Once the fluid is fully coupled to the disk, a ridge of uplifted fluid appears at the edge of the disk. Figure 4b shows a schematic of the fluid flow in the experiment as inferred from observations of particle motions in the fluid. Figure 5 displays photographs of the actual experiment. Although the ridge width and amplitude depend on the rpm of the disk, the ridge is typically 2–4 cm wide by 1–2 cm tall. At a some critical rpm the ridge disappears altogether, while at the maximum rpm, the hydrostatic pressure in the ridge eventually forces the fluid to flow in toward the shaft, inundating the disk. Finally, outside of the ridge a slight trough can often be observed.

For comparison, the same experiment was carried out with pure Karo corn syrup, known for being purely viscous with a Newtonian (albeit temperature-dependent) viscosity. The surface of the syrup was unaffected by the rotating disk, except at high rpm centrifugal acceleration created a slight parabolic uplift at the wall of the cylinder. Thus we can safely conclude that the uplift at the disk's edge in the experiment with CMC is due to viscoelasticity.

A crucial point about the applicability of viscoelasticity to deformation at transform faults is whether De equals $t_r \dot{\epsilon}_s$ (where $\dot{\epsilon}_s$ is the strain rate across a shear zone such as a transform fault) instead of, say, $t_r \Omega$ (Ω is analogous to the angular frequency of the tectonic plate rotating about its Euler pole). Only if the former is true will viscoelasticity be relevant at transform faults (because for a tectonic plate, $t_r \Omega \ll 1$). Although the thickness of the shear zone appears in the theoretical model, an experimental verification that the relevant De is proportional to $\dot{\epsilon}_s$ and not Ω is desirable. Thus we run the disk-cylinder experiment with CMC with disks of different size while maintaining the same R_d/H ratio. (The R_d/R_c ratio probably has no serious effect because the flow decays rapidly with radius r such that fluid motion ceases well before $r = R_c$; thus, in essence, there are negligible edge effects and R_c could effectively be infinite.) We assume the ridge first appears at some critical $De = De_c$ for all the trials. With different disks, we locate the Ω (i.e., the rpm) at which uplift first occurs. If $De = t_r \Omega$, then uplift should occur at the same rpm for all cases. Alternatively, if $De = t_r \dot{\epsilon}_s$, then since $\dot{\epsilon}_s \sim \Omega R_d / (R_c - R_d)$ depends on the size of the disk, a larger disk will require a lower rpm to create the ridge. The latter case in fact occurs: as the disk radius increases, a smaller Ω is required to generate the minimum uplift (Table 1). Therefore from an experimental perspective, $De = t_r \dot{\epsilon}_s$ is the relevant Deborah number.

TABLE 1. Disk Angular Frequency (rpm) at the First Appearance of the Ridge in the Disk-Cylinder Experiment for Different Disk Radii R_d and Ratios of Disk Radius to Fluid Depth R_d/H

R_d/H	R_d , cm	Frequency (at Onset of Ridge), rpm			
		Trial 1	Trial 2	Trial 3	Trial 4
1	4.7	22	20	20	19.5
1	6.0	14	14	13	13
1/2	4.7	30	29	30	30
1/2	6.0	22	19.5	19	19

The revolutions per minute (rpm) listed are not for the disk itself but for the low gear shaft on the Bodine motor.

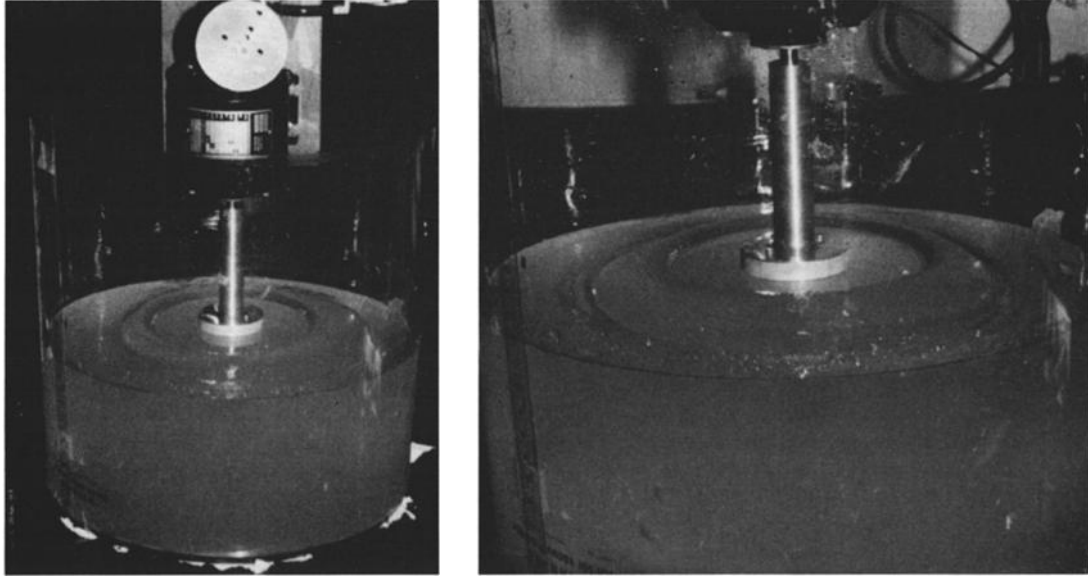


Fig. 5. Photograph of the disk-cylinder experiment with carboxymethylcellulose. See text for discussion.

THEORETICAL DESCRIPTION OF EXPERIMENT

To test the validity of the theoretical model, we present a cylindrical version of the model for the experiment described above. We do not intend to match the experiment exactly because a shear thinning rheology cannot be described by a second-order fluid which assumes a constant viscosity. A higher-order fluid [Tanner, 1985; Bird *et al.*, 1987] may be more appropriate; yet the flow theorems that allow us to use Newtonian velocity fields in the viscoelastic model are only valid for a second-order fluid. Thus we only seek to show that the theory qualitatively predicts the experimentally observed uplift.

We assume that the flow in the experiment is cylindrically axisymmetric, in which case the tangential component of the Stokes equation for an incompressible constant viscosity Newtonian fluid is

$$\frac{\partial}{\partial r} \frac{1}{r} \frac{\partial(rv)}{\partial r} + \frac{\partial^2 v}{\partial z^2} = 0 \quad (15)$$

where v is the tangential velocity. The solution to this equation with no slip boundary conditions at the base $z = 0$ and the wall of the cylinder $r = R_c$ is

$$v(r, z) = \sum_{n=1}^{\infty} A_n J_1(k_n r) \frac{\sinh(k_n z)}{\sinh(k_n H)} \quad (16)$$

where J_1 is a Bessel function of the first kind and first order, the k_n are the roots of the equation $J_1(kR_c) = 0$, and the A_n are the coefficients of the Bessel series. The boundary conditions at $z = H$ require that the tangential velocity $v = \Omega r$ for $0 \leq r \leq R_d$ (i.e., no slip beneath the disk) and $\partial v / \partial z = 0$ for $R_d \leq r \leq R_c$ (i.e., free slip between the disk edge and the cylinder wall). The coefficients A_n can be found numerically via collocation by truncating the series in (16) at $n = N$ and solving the linear set of N equations

$$\sum_{n=1}^N C_{mn} A_n = B_m, \quad m = 1, \dots, N \quad (17a)$$

where

$$C_{mn} = \begin{cases} J_1(k_n r_m) & 0 \leq r_m \leq R_d \\ J_1(k_n r_m) k_n \coth(k_n H) & R_d \leq r_m \leq R_c \end{cases}, \quad (17b)$$

$$B_m = \begin{cases} \Omega r_m & 0 \leq r_m \leq R_d \\ 0 & R_d \leq r_m \leq R_c \end{cases} \quad (17c)$$

and $r_m = (m - 1)R_c / (N - 1)$ are the radial collocation points. A truncation level of $N \geq 20$ creates a well-resolved solution for $v(r, z)$; yet $N \geq 40$ is required for the strain rates and viscoelastic stresses to be well resolved.

This solution for v is inserted into (2) with $\lambda_1 = \lambda_2 = \lambda < 0$, and the resulting stress components are substituted into the equation for vertical stress (i.e., the cylindrical analog to (8)) [Bird *et al.*, 1987]:

$$\frac{\partial}{\partial r} (P - \tau_{zz}) = \frac{\partial}{\partial r} (\tau_{rr} - \tau_{zz}) + \frac{\tau_{rr} - \tau_{\theta\theta}}{r} + \frac{\partial \tau_{rz}}{\partial z} \quad (18)$$

The indefinite integral of (18) over r yields the vertical uplift (in terms of stress) as a function of r ; this relation, evaluated near the surface, is shown in Figure 6. A sharp ridge is predicted to occur just inside of $r = R_d$, and a trough with slightly smaller amplitude occurs just outside the disk. Although both a ridge and a small trough occur in the experiment, both occur at $r > R_d$. However, the disk is rigid, which may cause secondary effects, such as the extrusion of fluid from under the disk. The theory at least predicts that a ridge and smaller trough occur near the edge of the disk. This correlates with the Quelleffekt and experiments to study the secondary flow in a disk-cylinder configuration (however, in these systems the disk extends to the cylinder wall; hence the effects leading to the trough are not observed). The theoretical model also adequately predicts stresses in the presence of secondary flow even though the theory does not account for secondary flow.

DISCUSSION

In summary, we have shown that because of the relatively high strain rates, potentially large Maxwell relaxation time, and finite deformation in the transform fault environment, nonlinear viscoelasticity may play an important role in the

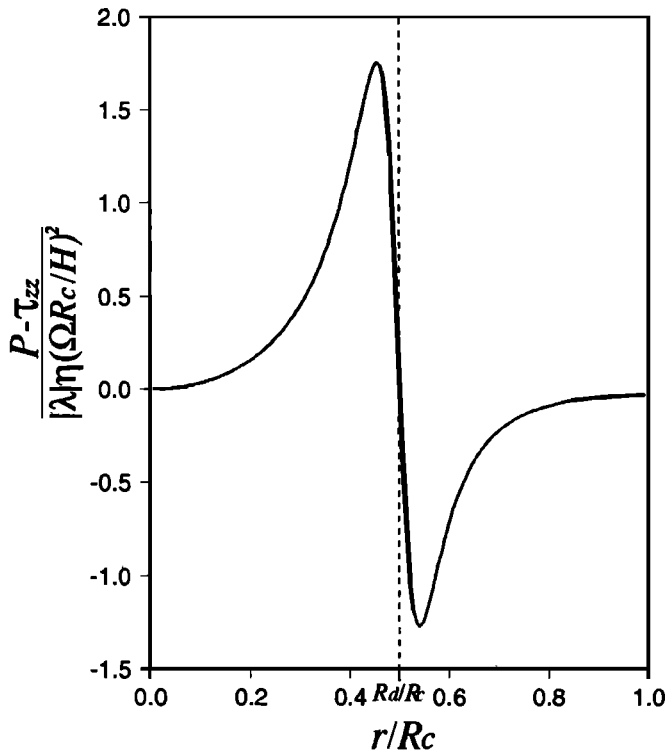


Fig. 6. Nondimensional uplift (in terms of stresses) versus dimensionless radius for the theoretical model of the disk-cylinder experiment. The curve is derived from the integration of (14) (with $R_d/R_c = 0.5$, $H/R_c = 1$ and the integration constant constrained such that no uplift occurs at $r = 0$) evaluated at $z = 0.95H$; this depth was chosen because at $z = H$ the velocity gradients are nearly discontinuous at $r = R_d$ (i.e., at $r/R_c = 0.5$) which compromises the validity of the second-order fluid approximation. The Bessel function series solution for the uplift is truncated at $n = 160$, whereas the solution is well resolved for $n \geq 40$. The vertical dashed line shows where $r = R_d$.

formation of transverse ridges. We have further demonstrated with both a simple theory and a laboratory experiment that nonlinear viscoelasticity can turn the purely horizontal motion of transform faults into vertical uplift characteristic of transverse ridges: not only does the uplift have the approximate shape and amplitude of a transverse ridge, it arises from dynamic yet nonbuoyant support, in accord with geophysical observations.

However, there are several caveats and drawbacks to our model that are worth enumerating. First, we must reiterate that the viscosities required for the viscoelastic mechanism to be significant may lead to excessive shear stress beneath the fault zone. Furthermore, the viscoelastic effect will be diminished if the high strain rates of the transform fault reduce the effective viscosity of ductile lithosphere beneath the fault through pseudo-plasticity or intense shear heating. Second, the theoretical model is two dimensional, inherently symmetric about the transform fault, and time independent. Across-fault asymmetries and monotonic along-strike variations in the transverse ridges may be accounted for by changes in elastic plate thickness due to age variations and offsets. However, the model presently cannot predict the often three-dimensional structure of the ridges, e.g., undulations along the ridge crests. Even so, it may be possible to explain these three-dimensional features by considering that the viscoelastic effect is very sensitive to the width of the transform shear zone and the viscosity of ductile lithosphere

in the vicinity of the transform fault (although, if the ductile lithosphere is pseudo-plastic or softened from shear heating, these two quantities are not necessarily independent). Any event which broadens the zone of transform shear, or lowers the effective viscosity of the mantle beneath the transform fault, may inhibit formation of a transverse ridge. The width of the shear zone may be very sensitive to the state of stress existing across a transform fault which can vary radically with transient changes in spreading direction from compressive to tensile. Furthermore, at slow-spreading ridges mantle flow beneath the ridge axis is believed to be highly nonuniform with mantle upwelling believed concentrated at regularly spaced points along the ridge axis [Whitehead *et al.*, 1984]. This should be accompanied by significant lateral variations in mantle temperature beneath the ridge axis. In the case where a center of mantle upwelling is situated close to a ridge transform intersection, this might sufficiently lower the effective viscosity to eliminate the viscoelastic effect and inhibit the formation of a transverse ridge for long periods of time.

These simple models also do not account for the vertical viscosity structure of the lithosphere and especially the asthenosphere where viscosity is low enough to possibly eliminate viscoelastic effects. However, the velocity and stress fields beneath the transform fault decay away within a depth approximately equal to the dominant horizontal wavelength of these fields (see (6a)) which is the typical width of the transform fault, between 1 and 10 km. Thus the important viscoelastic stresses are probably generated within a narrow region in the lower lithosphere.

Transverse ridges also do not occur at all transform faults: they are generally most pronounced at slow spreading centers. While this is contrary to our hypothesis that viscoelastic effects can cause transverse ridges (because De should theoretically be larger at a faster spreading ridge and thus cause greater viscoelastic stresses), fast spreading ridges have hotter, thinner lithospheres, effectively reducing the region in which viscoelastic deformation may occur. Furthermore, because of higher strain rates at fast spreading ridges, viscous flow will not predominate over brittle failure until considerably lower viscosities, nearer to the asthenosphere; thus the region where viscoelastic effects can occur may be confined to a much narrower region than for slower spreading ridges, and possibly eliminated altogether.

Nonlinear viscoelasticity does not obviate previous models of transverse ridges. We simply offer this effect as a possible explanation for an enigmatic phenomenon. Whether or not viscoelastic stresses are the cause of transverse ridges is perhaps a minor point; that they can cause the ridges is an important indication that a heretofore unexplored dynamic mechanism may be at play at narrow plate boundaries. Because of their high strain rates, large t_r (due to the high viscosity of the lithosphere), and finite deformation, narrow plate boundaries (not just transform faults) are good candidates for maintaining nonlinear viscoelastic phenomena.

Acknowledgments. We are especially grateful to John A. Whitehead, Jr., for helpful discussions and advice concerning both theoretical and laboratory efforts. We also wish to thank Pål Wessel for invaluable discussions regarding lithospheric flexure, Norman Sleep for constructive criticism, Cynthia Schnoes for photographs of the laboratory experiments, and Patrick V. Rossiello of the Aqualon Company, who provided helpful information and complementary samples of CMC. This work was supported by the W. M. Keck Marine Geodynamics program at the Woods Hole Oceanographic Institution (WHOI); the majority of

this study was performed during the first author's postdoctoral fellowship at WHOI.

REFERENCES

- Abrams, L. J., R. S. Detrick, and P. J. Fox, Morphology and crustal structure of the Kane Fracture Zone transverse ridge, *J. Geophys. Res.*, *93*, 3195-3210, 1988.
- Aqualon Company, *Aqualon Cellulose Gum, Sodium Carboxymethylcellulose: Physical and Chemical Properties*, Wilmington, Del., 1989.
- Beaumont, C., The evolution of sedimentary basins on a viscoelastic lithosphere, *Geophys. J. R. Astron. Soc.*, *55*, 471-497, 1976.
- Bird, R. B., W. E. Stewart, and E. N. Lightfoot, *Transport Phenomena*, John Wiley, New York, 1960.
- Bird, R. B., R. C. Armstrong, and O. Hassager, *Dynamics of Polymeric Liquids* vol. 1, Wiley Interscience, New York, 1987.
- Böhme, G., R. Voß, and W. Warnecke, Die freie Oberfläche einer Flüssigkeit über einer rotierenden Scheibe, *Rheol. Acta*, *24*, 22-33, 1985.
- Bonatti, E., Vertical tectonism in oceanic fracture zones, *Earth Planet. Sci. Lett.*, *37*, 369-379, 1978.
- Bonatti, E., and A. Chermak, Formerly emerging crustal blocks in the equatorial Atlantic, *Tectonophysics*, *72*, 165-180, 1981.
- Bonatti, E., and J. Honnorez, Non-spreading crustal blocks at the Mid-Atlantic Ridge, *Science*, *174*, 1329-1331, 1971.
- Bonatti, E., and J. Honnorez, Sections of the Earth's crust in the equatorial Atlantic, *J. Geophys. Res.*, *81*, 4104-4116, 1976.
- Bonatti, E., R. Sartori, and A. Boersma, Vertical crustal movements at the Vema Fracture Zone in the Atlantic: Evidence from dredged limestones, *Tectonophysics*, *91*, 213-223, 1983.
- Cathles, L. M., III, *The Viscosity of the Earth's Mantle*, Princeton University Press, Princeton, N. J., 1975.
- Cochran, J. R., Gravity and magnetic investigations in the Guiana Basin, western equatorial Atlantic, *Geol. Soc. Am. Bull.*, *84*, 3249-3268, 1973.
- De Bremaecker, J.-C., *Geophysics: The Earth's Interior*, John Wiley, New York, 1985.
- Detrick, R. S., and G. M. Purdy, The crustal structure of the Kane Fracture Zone from seismic refraction studies, *J. Geophys. Res.*, *85*, 3759-3777, 1980.
- Dick, H. J. B., H. Schouten, D. G. Gallo, P. S. Meyer, H. Bergh, R. Tyce, P. Patriat, T. M. Johnson, J. Snow, and A. Fisher, Tectonic evolution of the Atlantis II Fracture Zone, in *Proceedings of the Ocean Drilling Program, Scientific Results 118*, edited by P. T. Robinson and R. Von Herzen, Texas A & M Press, College Station, Tex., 1990.
- Fisher, R. L., and J. G. Sclater, Tectonic evolution of the southwest Indian Ocean since the mid-Cretaceous: Plate motions and stability of the pole of Antarctica/Africa for at least 80 m.y., *Geophys. J. R. Astron. Soc.*, *73*, 553-576, 1983.
- Forsyth, D., and S. Uyeda, On the relative importance of the driving forces of plate tectonics, *Geophys. J. R. Astron. Soc.*, *43*, 163-200, 1975.
- Fox, P. J., and D. G. Gallo, A tectonic model for ridge-transform-ridge plate boundaries: Implications for the structure of oceanic lithosphere, *Tectonophysics*, *104*, 205-242, 1984.
- Garner, F. H., and A. H. Nissan, Rheological properties of high-viscosity solutions of long molecules, *Nature*, *158*, 634-635, 1946.
- Giesekus, H., Die simultane Translations- und rotationsbewegung einer Kugel in einer elastoviskosen Flüssigkeit, *Rheol. Acta*, *3*, 59-71, 1963.
- Hill, C. T., Nearly viscometric flow of viscoelastic fluids in the disk and cylinder system, II, Experimental, *Trans. Soc. Rheol.*, *16*, 213-245, 1972.
- Honnorez, J., E. Bonatti, C. Emiliani, P. Bronnimann, M. A. Furrer, and A. A. Meyeroff, Mesozoic limestones from the Vema offset zone, *Earth Planet. Sci. Lett.*, *26*, 8-12, 1975.
- Karson, J. A., and H. J. B. Dick, Tectonics of ridge-transform intersections at the Kane Fracture Zone, *Mar. Geophys. Res.*, *6*, 51-98, 1983.
- Kramer, J. M., and M. W. Johnson, Jr., Nearly viscometric flow in the disk and cylinder system, I, Theoretical, *Trans. Soc. Rheol.*, *16*, 197-212, 1972.
- Louden, K. E., and D. W. Forsyth, Crustal structure and isostatic compensation near the Kane Fracture Zone from topography and gravity measurements, I, Spectral analysis approach, *Geophys. J. R. Astron. Soc.*, *68*, 725-750, 1982.
- Macdonald, K. C., D. A. Castillo, S. P. Miller, P. J. Fox, K. A. Kastens, and E. Bonatti, Deep-tow studies of the Vema Fracture Zone, 1, Tectonics of a major slow slipping transform fault and its intersection with the Mid-Atlantic Ridge, *J. Geophys. Res.*, *91*, 3334-3354, 1986.
- Malvern, L. E., *Introduction to the Mechanics of a Continuous Medium*, Prentice-Hall, Englewood Cliffs, N. J., 1969.
- Man, C.-S., and Q.-X. Sun, On the significance of normal stress effects in the flow of glaciers, *J. Glaciol.*, *33*, 268-273, 1987.
- McTigue, D. F., S. L. Passman, and S. J. Jones, Normal stress effects in the creep of ice, *J. Glaciol.*, *31*, 120-126, 1985.
- Melson, W. G., and G. Thompson, Petrology of a transform fault zone and adjacent ridge segments, *Philos. Trans. R. Soc. London Ser. A*, *268*, 423-441, 1971.
- Metzner, A. B., Non-Newtonian technology: Fluid mechanics, mixing and heat transfer, *Adv. Chem. Eng.*, *1*, 77-153, 1956.
- Nirschl, J. P., and W. E. Stewart, Computation of viscoelastic flow in a cylindrical tank with a rotating lid, *J. Non-Newtonian Fluid Mech.*, *16*, 233-250, 1984.
- Peltier, W. R., Dynamics of the ice age Earth, *Adv. Geophys.*, *24*, 1-146, 1982.
- Pipkin, A. C., and R. S. Rivlin, Normal stresses in flow through tubes of non-circular cross-section, *Z. Angew. Math. Phys.*, *14*, 738-742, 1963.
- Ranalli, G., *Rheology of the Earth*, Allen and Unwin, Winchester, Mass., 1987.
- Robb, J. M., and M. F. Kane, Structure of the Vema Fracture Zone from gravity and magnetic intensity profiles, *J. Geophys. Res.*, *80*, 4441-4445, 1975.
- Savage, S. B., The mechanics of rapid granular flows, *Adv. Appl. Mech.*, *24*, 289-366, 1984.
- Schubert, G., and D. L. Turcotte, One-dimensional model of shallow mantle convection, *J. Geophys. Res.*, *77*, 945-951, 1972.
- Sclater, J. G., H. Dick, I. O. Norton, and D. Woodruffe, Tectonic structure and petrology of the Antarctic plate boundary near the Bouvet triple junction, *Earth Planet. Sci. Lett.*, *37*, 393-400, 1978.
- Searle, R. C., and A. S. Laughton, Sonar studies of the Mid-Atlantic Ridge and Kurchatov Fracture Zone, *J. Geophys. Res.*, *82*, 5313-5328, 1977.
- Sevringhaus, J. P., and K. C. Macdonald, High inside corners at ridge-transform intersections, *Mar. Geophys. Res.*, *9*, 353-367, 1988.
- Sleep, N. L., and S. Biehler, Topography and tectonics at the intersections of fracture zones with central rifts, *J. Geophys. Res.*, *75*, 2748-2752, 1970.
- Tanner, R. I., *Engineering Rheology*, Clarendon, Oxford, United Kingdom, 1985.
- Tucholke, B. E., and H. Schouten, Kane Fracture Zone, *Mar. Geophys. Res.*, *10*, 1-39, 1988.
- Turcotte, D. L., and G. Schubert, *Geodynamics: Applications of Continuum Physics to Geological Problems*, John Wiley, New York, 1982.
- Watts, A. B., G. D. Karner and M. S. Steckler, Lithospheric flexure and the evolution of sedimentary basins, *Philos. Trans. R. Soc. London, Ser. A*, *305*, 249-281, 1982.
- Wessel, P., Thermal bending stresses in young oceanic lithosphere: Implications for vertical motions on transform faults (abstract), *Eos Trans. AGU*, *71*, 1597-1598, 1990.
- Whitehead, J. A., Jr., H. J. B. Dick, and H. Schouten, A mechanism for magmatic accretion under spreading centers, *Nature*, *312*, 146-148, 1984.
- Yuen, D. A., R. Sabadini, and E. V. Boschi, Viscosity of the lower mantle as inferred from rotational data, *J. Geophys. Res.*, *87*, 10,745-10,762, 1982.

D. Bercovici, Department of Geology and Geophysics, School of Ocean and Earth Science and Technology, University of Hawaii, Honolulu, HI 96822.

H. J. B. Dick, Department of Geology and Geophysics, Woods Hole Oceanographic Institution, Woods Hole, MA 02543.

T. P. Wagner, Department of Earth, Atmospheric and Planetary Sciences, Massachusetts Institute of Technology, Cambridge, MA 02139.

(Received September 3, 1991;
revised April 8, 1992;
accepted April 16, 1992.)